

Transport properties of proximitized double quantum dots

G. Górski^{1,*} and K. Kucab^{1,†}

¹*Institute of Physics, College of Natural Sciences, University of Rzeszów,
ul. Pigonia 1, PL-35-310 Rzeszów, Poland*

(Dated: March 23, 2022)

We study the sub-gap spectrum and the transport properties of a double quantum dot coupled to metallic and superconducting leads. The coupling of both quantum dots to the superconducting lead induces a non-local pairing in both quantum dots by the Andreev reflection processes. Additionally, we obtain two channels of Cooper pair tunneling into a superconducting lead. In such a system, the direct tunneling process (by one of two dots) or the crossed tunneling process (by both quantum dots at the same time) is possible. We consider the dependence of the Andreev transmittance on an inter-dot tunneling amplitude and the coupling between a quantum dot and the superconducting lead. We also consider the occurrence of interferometric Fano-type line shapes in the linear Andreev conductance spectra.

Keywords: double quantum dots, Andreev scattering, superconducting proximity effect, Fano effect

I. INTRODUCTION

The rapid development of electronics results in research of the transport properties of different types of heterostructures consisting of nano-objects such as the quantum dots or nanowires. One of the directions of interest is the system consisting of double quantum dots (DQD) placed between superconducting, magnetic or metallic leads [1–30].

For a system with a DQD coupled to two metallic or ferromagnetic electrodes [1–3, 5, 6, 10, 14], we observe the coexistence of Kondo [31] and Fano [32] effects. The connection between one quantum dot (QD₁) and metallic electrodes leads to the widening of a dot level. When the second dot (QD₂) is side coupled to the first one, there is a possibility to obtain the Fano-like asymmetric line shapes in the linear conductance [3–7, 14] which are obtained as a result of the interference between discrete QD₂ level with a broad band of QD₁. Additionally, for interacting dots, one obtains a two-stage Kondo effect [2, 3, 14, 29, 30]. The Fano destructive interference partially suppresses the Kondo resonance.

For the case of one quantum dot attached to one superconducting (SC) and one normal metallic (N) contact (N-QD-SC system), the propagation of a Cooper pair into SC lead and a hole reflection into a metallic lead (Andreev reflection process) occurs in the system [33, 34]. The connection of second QD into the N-QD-SC system causes the competition between the Andreev and Fano effect [4, 8, 15, 26, 28]. Other options of DQD with SC and N leads connection are also considered, e.g. connection of the first dot to two metallic leads and the second dot to the SC lead [11, 12, 19, 23, 25]. In such systems, there are possible both the normal electron transfers (when the single electron transfers between both normal metallic electrodes) and direct (DAR) and crossed (CAR) Andreev

reflections (when electrons of the Cooper pair tunnel into SC lead and the holes tunnel to the same (DAR) or the second (CAR) metallic lead). The hybrid DQD structure can be used as a Cooper pair splitter if each QD is connected with separate metallic leads [20, 21, 24].

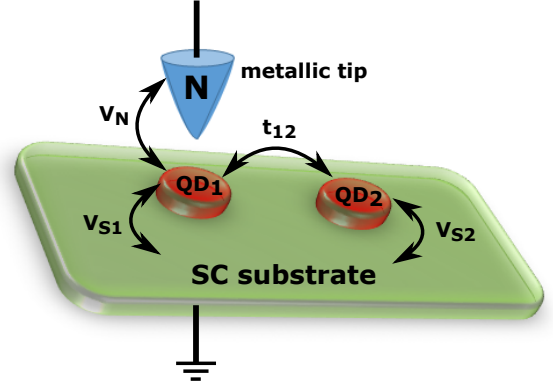


FIG. 1. Schematic representation of the double quantum dot system. The metallic lead is coupled to the first quantum dot (QD₁), the superconductor substrate is attached to both quantum dots (QD₁ and QD₂).

In this paper we consider a system consisted of two quantum dots embedded in a superconducting substrate (see Fig. 1). We assume that a metallic lead is connected with one of these dots. Such a system can be realized experimentally by the use of scanning tunneling microscopy (STM) measurements of metallic atoms (e.g. Fe atoms) embedded in the superconducting substrate (e.g. Pb substrate) by the use of metallic tip. The STM-based single-atom manipulations technique is currently widely used for the detection of Majorana bound states in metallic chains [35–39]. This method allows for precise positioning of atoms on the substrate and for the local determination of spectral and transport properties of individual atoms [39]. In the system considered by

* ggorski@ur.edu.pl

† kkucab@ur.edu.pl

us, the neighborhood of SC substrate with QDs, by the proximity effect, generates the Andreev states both on QD₁ and on QD₂. The coupling of both QDs with SC lead causes that the Cooper pair can tunnel to the SC lead via one of two dots (direct tunneling) or via both dots at the same time (crossed tunneling). Our aim is to analyze the spectral and transport properties of the quantum dot QD₁ depending on its coupling with proximitized QD₂. These results are important in the context of the distinction between the coupling of QD with trivial Andreev bound states and topological Majorana bound states [40].

This work is structured as follows. In Sec. II we introduce the microscopic model which describes the system considered by us. In this section, we introduce the relations describing the transport properties of the system. In Sec. III we present the numerical results for the local density of states and for the Andreev transmission coefficient. We also analyze the influence of our model parameters on the observed Fano-type line shapes of Andreev transmittance. Finally, the conclusions can be found in Sec. IV

II. THE MODEL

We consider the system consisted of two quantum dots embedded in the superconducting substrate (see Fig. 1). The use of a metallic tip allows us to obtain the current characteristics of the system. We assume that the QDs are connected to the same SC leads, so the difference of the superconducting phases does not occur and the Josephson current is not observed. The total Hamiltonian of our setup has the following form:

$$H = \sum_{i\sigma} \varepsilon_i d_{i\sigma}^\dagger d_{i\sigma} + \sum_{\sigma} t_{12} (d_{1\sigma}^\dagger d_{2\sigma} + h.c.) \quad (1)$$

$$+ \sum_{\mathbf{k}\sigma\beta} \xi_{\mathbf{k}\beta} c_{\mathbf{k}\sigma\beta}^\dagger c_{\mathbf{k}\sigma\beta} - \sum_{\mathbf{k}} (\Delta c_{\mathbf{k}\uparrow S}^\dagger c_{-\mathbf{k}\downarrow S}^\dagger + h.c.)$$

$$+ \sum_{\mathbf{k}\sigma} (V_{\mathbf{k}N} d_{1\sigma}^\dagger c_{\mathbf{k}\sigma N} + h.c.) + \sum_{\mathbf{k}i\sigma} (V_{\mathbf{k}Si} d_{i\sigma}^\dagger c_{\mathbf{k}\sigma S} + h.c.),$$

where $d_{i\sigma}^\dagger$ ($d_{i\sigma}$) are the creation (annihilation) operators of an electron with spin σ at QD_{*i*} ($i = 1, 2$), ε_i is the energy level of QD_{*i*}, t_{12} is the inter-dot tunneling amplitude, $c_{\mathbf{k}\sigma\beta}^\dagger$ ($c_{\mathbf{k}\sigma\beta}$) denote the creation (annihilation) operators of an electron with momentum \mathbf{k} and spin σ in the metallic tip ($\beta = N$) or in the superconducting substrate ($\beta = S$), $\xi_{\mathbf{k}\beta} = \epsilon_{\mathbf{k}\beta} - \mu_\beta$ is an energy dispersion of the lead β measured with respect to the electrochemical potentials μ_β . We assume that $\mu_S = 0$ and $\mu_N = eV$. $V_{\mathbf{k}N}$ is the tunneling amplitude between the QD₁ and the metallic tip, and $V_{\mathbf{k}Si}$ is the tunneling amplitude between the *i*-dot and superconducting substrate. Δ is the superconducting energy gap.

The coupling between QDs and an SC substrate leads to the Andreev reflection processes [33], where taking an electron from a metallic lead causes the injection of a Cooper pair into the SC lead and the reflection of a hole into a metallic lead. In the considered system, for $V_{\mathbf{k}S2} \neq 0$, the direct tunneling is possible when the injection of the Cooper pair occurs from one of two QDs, or crossed tunneling is possible when the Cooper pair creates one electron from each dot.

We focus on the Andreev transport regime, so we use the $\Delta \rightarrow \infty$ limit [20, 41, 42]. In a wide-bandwidth limit, we introduce the coupling constant between QD₁ and a metallic lead $\Gamma_N = 2\pi \sum |V_{\mathbf{k}N}|^2 \delta(\omega - \xi_{\mathbf{k}N})$, and the coupling constant between QD_{*i*} and superconducting substrate $\Gamma_{Si} = 2\pi \sum |V_{\mathbf{k}Si}|^2 \delta(\omega - \xi_{\mathbf{k}S})$. The effective Hamiltonian takes on the following form:

$$H_{\text{eff}} = \sum_{i\sigma} \varepsilon_i d_{i\sigma}^\dagger d_{i\sigma} + \sum_{\sigma} t_{12} (d_{1\sigma}^\dagger d_{2\sigma} + h.c.) \quad (2)$$

$$+ \sum_{\mathbf{k}\sigma} \xi_{\mathbf{k}N} c_{\mathbf{k}\sigma N}^\dagger c_{\mathbf{k}\sigma N} + \sum_{\mathbf{k}\sigma} (V_{\mathbf{k}N} d_{1\sigma}^\dagger c_{\mathbf{k}\sigma N} + h.c.)$$

$$- \sum_i \frac{\Gamma_{Si}}{2} (d_{i\uparrow}^\dagger d_{i\downarrow}^\dagger + h.c.) + \sum_i \frac{\Gamma_{S\bar{i}}}{2} (d_{i\uparrow}^\dagger d_{i\downarrow}^\dagger + h.c.),$$

where $\bar{i} = 2$ for $i = 1$ and $\bar{i} = 1$ for $i = 2$, $\Gamma_{Si}(\Gamma_{S\bar{i}})$ is the direct (cross) coupling between *i*-dot and the SC substrate. We assume that $\Gamma_{S12} = \Gamma_{S21} = \sqrt{\Gamma_{S1}\Gamma_{S2}}$ [20, 25, 42].

Using the equation of motion method, we obtain the matrix of Green's functions $\mathcal{G}(\omega) = \langle\langle \Psi; \Psi^\dagger \rangle\rangle$, where $\Psi^\dagger = (d_{1\uparrow}, d_{1\downarrow}, d_{2\uparrow}, d_{2\downarrow})$, in the following notation

$$\mathcal{G}^{-1}(\omega) = \begin{pmatrix} \omega - \varepsilon_1 + \frac{i\Gamma_N}{2} & \frac{\Gamma_{S1}}{2} & -t_{12} & \frac{-\Gamma_{S12}}{2} \\ \frac{\Gamma_{S1}}{2} & \omega + \varepsilon_1 + \frac{i\Gamma_N}{2} & \frac{-\Gamma_{S12}}{2} & t_{12} \\ -t_{12} & \frac{-\Gamma_{S12}}{2} & \omega - \varepsilon_2 & \frac{\Gamma_{S2}}{2} \\ \frac{-\Gamma_{S12}}{2} & t_{12} & \frac{\Gamma_{S2}}{2} & \omega + \varepsilon_2 \end{pmatrix}. \quad (3)$$

In the SC atomic limit, $\Gamma_N \rightarrow 0$, the Green's functions

are characterized by four poles

$$\varepsilon_{A1} = 1/\sqrt{2}\sqrt{A + \sqrt{A^2 - 4B}},$$

$$\varepsilon_{A2} = -1/\sqrt{2}\sqrt{A + \sqrt{A^2 - 4B}},$$

$$\varepsilon_{A3} = 1/\sqrt{2}\sqrt{A - \sqrt{A^2 - 4B}},$$

$$\varepsilon_{A4} = -1/\sqrt{2}\sqrt{A - \sqrt{A^2 - 4B}} \quad (4)$$

where $A = \varepsilon_1^2 + \varepsilon_2^2 + (\frac{\Gamma_{S1} + \Gamma_{S2}}{2})^2 + 2t_{12}^2$ and $B = (\varepsilon_1\varepsilon_2 - t_{12}^2)^2 + (\frac{\varepsilon_1\Gamma_{S2} + \varepsilon_2\Gamma_{S1}}{2} + \Gamma_{S12}t_{12})^2$. These poles correspond to four Andreev resonances. The non-zero value of Γ_N causes the broadening of these resonances. The generation of four Andreev states is related to the fact, that the proximity effect generates the Andreev states on both quantum dots. The generation of Andreev states on QD₁ is related to the direct coupling of the QD₁ with the SC lead. For this quantum dot the ε_{A1} and ε_{A2} states are dominant. For QD₂ we have two methods of generation of the Andreev states, (i) the direct one for $\Gamma_{S2} \neq 0$; (ii) the indirect one (via QD₁) for $\Gamma_{S2} = 0$ and $t_{12} \neq 0$. For this quantum dot ε_{A3} and ε_{A4} states dominate.

The properties of nanoscopic systems can be analyzed experimentally using the current characteristics, especially the zero-bias differential conductance. The current flowing from the N lead can be calculated using the following equation [43–45]

$$I_N = -e \frac{d}{dt} \langle \sum_{k\sigma} c_{k\sigma N}^\dagger c_{k\sigma N} \rangle \quad (5)$$

$$= -\frac{2e\Gamma_N}{h} \text{Im} \int [2f(\omega - \mu_N) \mathcal{G}_{11}^r(\omega) + \mathcal{G}_{11}^<(\omega)] d\omega$$

where $\mathcal{G}^r(\mathcal{G}^<)$ are the retarded (lesser) Green's functions, respectively, and $f(\omega)$ is the Fermi distribution function.

The total current is the sum of the normal and Andreev currents. At low temperatures, the normal current, when an electron moves from N lead to SC lead, is realized for $eV \geq \Delta$. For $eV \leq \Delta$ in the N-QD-SC system, we observe the Andreev current arising when an electron from N lead pairs with a second electron with opposite spin and as the Cooper pair they are tunneling to the SC lead and simultaneously, a hole with opposite spin is reflected back to the N lead [33, 46]. In our N-DQD-SC system, with $\Gamma_{S1} \neq 0$ and $\Gamma_{S2} \neq 0$, the Cooper pair can tunnel to the SC lead via one of two dots (direct tunneling) or via both dots at the same time (crossed tunneling).

For $\Delta \rightarrow \infty$ in our system there occurs the Andreev current only, so the relation describing the current I_N has the following form [8, 44]:

$$I_N = \frac{e}{h} \int T_A(\omega) [f(\omega - \mu_N) - f(\omega + \mu_N)] d\omega \quad (6)$$

where

$$T_A(\omega) = 2\Gamma_N^2 |\mathcal{G}_{12}^r(\omega)|^2 \quad (7)$$

is the total Andreev transmittance. The maximum of T_A value is equal to 2. The Andreev transmittance is always symmetric, $T_A(\omega) = T_A(-\omega)$, because the anomalous Andreev scattering involves both the particle and hole degrees of freedom.

The knowledge of an Andreev transmittance allows us

to calculate the zero-bias differential conductance as

$$G_A(V=0) = \partial I_N / \partial V|_{V \rightarrow 0} \quad (8)$$

$$= \frac{2e^2}{h} \int T_A(\omega) \left[-\frac{\partial f(\omega)}{\partial \omega} \right] d\omega.$$

At low temperatures, this equation can be simplified as follows:

$$G_A(V=0) = \frac{2e^2}{h} T_A(0). \quad (9)$$

III. RESULTS

In this section, we present the numerical results for the spectral density of QDs and the Andreev transmittance. As a unit of energy we assume the coupling parameter between QD₁ and SC substrate ($\Gamma_{S1} = 1$). The computations were carried out at $T = 0$.

A. Spectral density

The normalized spectral density of a quantum dot is defined as:

$$A_i(\omega) = -\frac{\Gamma_N}{2} \text{Im} \langle\langle d_{i\uparrow}; d_{i\uparrow}^\dagger \rangle\rangle_\omega. \quad (10)$$

With such defined normalized spectral density, the maximum value of $A_1(\omega)$ is equal to 1.

In Fig. 2 we present the normalized spectral density of QD₁ (top panel) and QD₂ (bottom panel) as a function of the inter-dot tunneling amplitude (t_{12}) and for different values of the coupling parameter Γ_{S2} . For the computations, we assumed an equal energy level for QDs ($\varepsilon_1 = \varepsilon_2 = 0$), which is consistent with a chemical level of SC lead.

For $\Gamma_{S2} = 0$ (left panel) we obtain the system with a side-coupled QD₂, which is not directly coupled to the leads (metallic or superconducting) [4, 8, 10, 13, 15, 16]. In this case, the dependence of spectral density for QD₁ and QD₂ is symmetric ($A_i(\omega) = A_i(-\omega)$). We also observe the symmetry of spectral density as a function of the inter-dot tunneling amplitude with respect to $t_{12} = 0$. As Barański and Domański shown [8], in this T-shape configuration the Fano-type resonances and antiresonances localized near $\pm\varepsilon_2$ are obtained. The Fano resonances are characterized by a typical asymmetric line shape and are obtained if a broad spectrum interferes with a discrete level. In our system, a broad QD₁ spectrum, resulting from coupling QD₁ with metallic lead, interferes with discrete QD₂ level. As a result of Fano type quantum interference, for $\omega = \varepsilon_2$ we obtain the spectral density $A_1(\omega = \varepsilon_2) = 0$ for all values of $t_{12} \neq 0$. The location of this antiresonance also does not depend on ε_1 . At strong inter-dot tunneling ($t_{12} > \Gamma_N$), both for $A_1(\omega)$ and $A_2(\omega)$, one can observe four resonance states

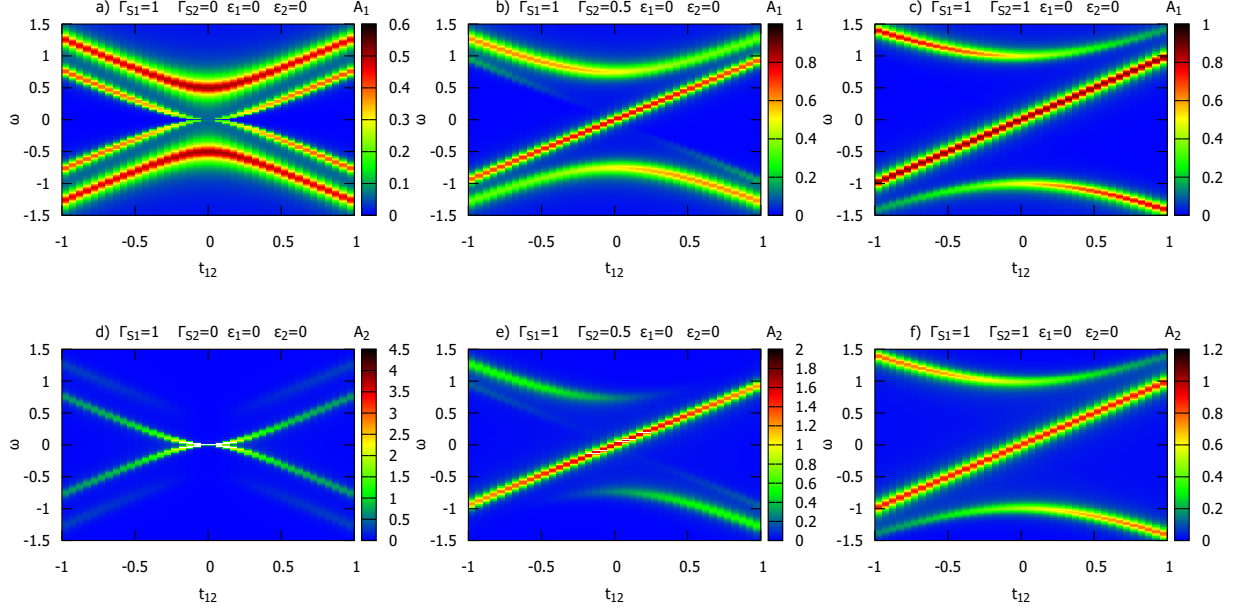


FIG. 2. The normalized spectral density of quantum dots (for QD₁ - top panel, and for QD₂ - bottom panel) as a function of the inter-dot tunneling amplitude t_{12} and for different values of the coupling parameter Γ_{S2} . Other parameters are $\varepsilon_1 = \varepsilon_2 = 0$, $\Gamma_{S1} = 1$ and $\Gamma_N = 0.25$.

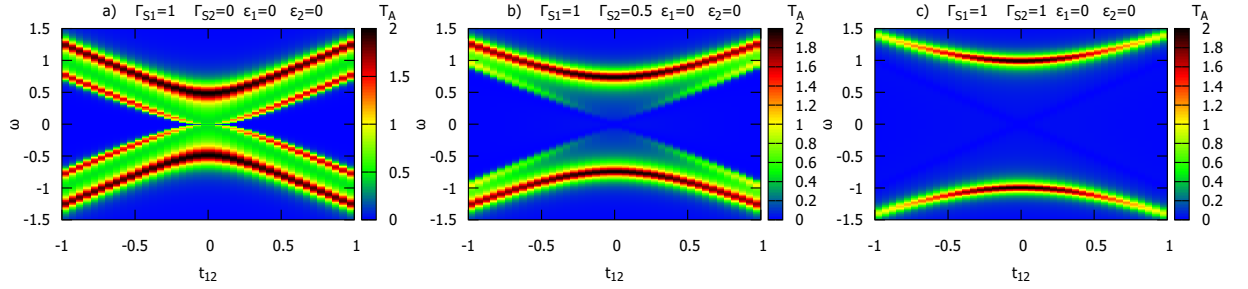


FIG. 3. The Andreev transmittance as a function of the inter-dot tunneling amplitude t_{12} , and for different values of the coupling parameter Γ_{S2} . Other parameters are $\varepsilon_1 = \varepsilon_2 = 0$, $\Gamma_{S1} = 1$ and $\Gamma_N = 0.25$.

localized near energies ε_{Ai} (see Eq. 4), which come from a direct Andreev effect for QD₁ and from an indirect Andreev effect for QD₂ [8]. For $\varepsilon_1 = \varepsilon_2 = 0$ two outer states (localized near ε_{A1} and ε_{A2}) dominate for $A_1(\omega)$, while two inner states (localized near ε_{A3} and ε_{A4}) dominate for $A_2(\omega)$.

The finite value of coupling between QD₂ and SC lead (middle and right panel of Fig. 2) causes a direct induction of pairing on QD₂. In this case, despite the dots energies which are equal to 0, the symmetry breaking of $A_i(\omega)$ is observed, whereas one can observe the $A_i(\omega, t_{12}) = A_i(-\omega, -t_{12})$ dependence. The outer Andreev states are still highly visible, and their location depends both on Γ_{S1} and Γ_{S2} . For the inner states, we obtain a strong peak near ε_{A3} and very weak peak near ε_{A4} . The non-zero value of Γ_{S2} causes that we do not observe

the Fano-type line shape of $A_1(\omega)$ ($A_1(\omega = \varepsilon_2) \neq 0$). For identical quantum dots with $\varepsilon_1 = \varepsilon_2$, which are characterized by an identical coupling with SC substrate $\Gamma_{S1} = \Gamma_{S2}$, we obtain three-center structure with one pair of Andreev resonances localized near ε_{A1} and ε_{A2} , and with strong resonance near $\varepsilon_2 + t_{12}$ (see right panel of Fig. 2).

B. Andreev transmittance

The dependence of Andreev transmittance (Eq. 7) as a function of inter-dot tunneling amplitude t_{12} is shown in Fig. 3. In the case of side-coupled QD₂ ($\Gamma_{S2} = 0$ and $t_{12} \neq 0$), two pairs of resonance states are visible in Andreev transmittance (see Fig. 3(a)) near $\omega = \varepsilon_{Ai}$. The

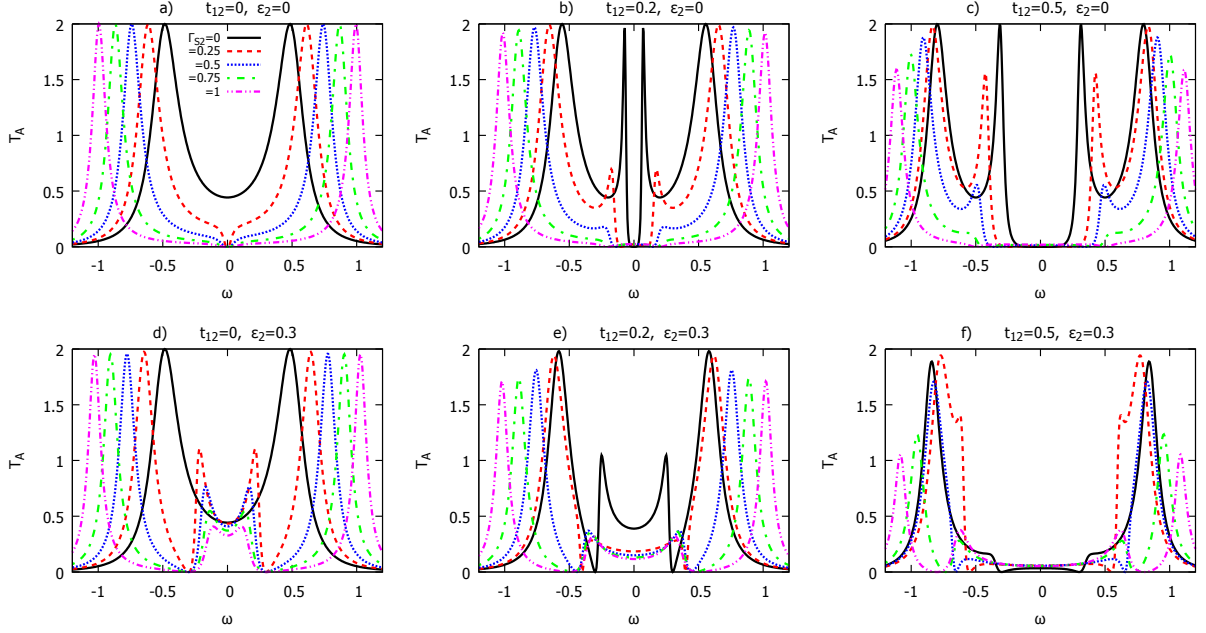


FIG. 4. The Andreev transmittance as a function of the coupling parameter Γ_{S2} and for different values of the inter-dot tunneling amplitude t_{12} and ε_2 . Other parameters are $\varepsilon_1 = 0$, $\Gamma_{S1} = 1$ and $\Gamma_N = 0.25$.

broad resonances are obtained for $\omega = \varepsilon_{A1}$ and $\omega = \varepsilon_{A2}$ and the narrow resonances are obtained for $\omega = \varepsilon_{A3}$ and $\omega = \varepsilon_{A4}$. Taking into account the coupling between QD₂ and a superconducting lead ($\Gamma_{S2} \neq 0$), one obtains the extinction of inner Andreev transmittance resonances (see Figs 3(b) and (c)). The increase of Γ_{S2} causes the shift of Andreev transmittance resonances localized near ε_{A1} and ε_{A2} towards higher energies. Additionally, these resonances become narrower. For the identical coupling of quantum dots with SC substrate, $\Gamma_{S1} = \Gamma_{S2}$, we obtain the total extinction of inner Andreev transmittance resonances (see Fig 3 (c)).

Now we will discuss the influence of the hybridization parameter Γ_{S2} on the Andreev transmittance (Fig. 4). In our analysis we consider the system of two QDs with equal energy $\varepsilon_1 = \varepsilon_2 = 0$ (top panel) and with different energies $\varepsilon_1 = 0$ and $\varepsilon_2 = 0.3$ (bottom panel). For $\Gamma_{S2} = 0$ (solid black line) we obtain the double QDs coupled in a T-shape configuration with metallic and superconducting lead [4, 8, 15]. As Barański and Domański [8] shown, in this configuration, for small $t_{12} \ll \Gamma_N$ one can obtain the Fano-type line shapes of Andreev transmittance. At high values of t_{12} , the Fano-type features disappear, evolving into the new quasi-particle peaks. Additional peaks can be interpreted as the Andreev peaks being a consequence of the indirect proximity effect induced by QD₁ on the side-attached QD₂. In this configuration, generally, for all values of $t_{12} \neq 0$, one obtains the $T_A(\varepsilon_2) = T_A(-\varepsilon_2) = 0$ dependence.

For a double quantum dot system, the Fano resonance is molded by the coupling of a narrow level related to QD₂, and a broad level related to QD₁. In the case of

direct coupling of QD₂ with SC lead $\Gamma_{S2} \neq 0$, as a result of proximity effect, there are created the narrow resonance Andreev levels on QD₂. In this case, we obtain the zero-value of Andreev transmittance (Fano dip) for energy value equal to

$$\varepsilon_F = \pm \sqrt{\varepsilon_2^2 + \frac{2t_{12}\Gamma_{S1}\varepsilon_2 + \Gamma_{S2}t_{12}^2}{\Gamma_{S1}}}. \quad (11)$$

As we have shown in Fig. 4 (a) and (d), the zeroing of Andreev transmittance ($T_A(-\varepsilon_F) = T_A(\varepsilon_F) = 0$) does not require $t_{12} \neq 0$. At $t_{12} = 0$ and $\Gamma_{S2} \neq 0$, the zero value of Andreev transmittance is obtained for $\varepsilon_F = \pm \varepsilon_2$, while for $t_{12} \neq 0$ we obtain that ε_F is not constant for a given ε_2 but it also depends on Γ_{S1} , Γ_{S2} , Γ_{S12} and t_{12} (see Fig. 4 (b), (c), (e) and (f)).

For QDs which do not interact directly ($t_{12} = 0$), the increase of Γ_{S2} causes the broadening of an effective value of the coupling parameter $\Gamma_{S\text{eff}} = \Gamma_{S1} + \Gamma_{S2}$, and as the effect, it causes the shift of Andreev resonances localized near $\omega = \varepsilon_{A1}$ and $\omega = \varepsilon_{A2}$, towards higher energy levels (see Fig. 4 (a) and (d)). In this case, the maximum of Andreev transmittance is close to 2. For $t_{12} \neq 0$ the increase of Γ_{S2} causes the decreasing of the maximum value of Andreev transmittance ($T_A(\varepsilon_{A1}) < 2$ and $T_A(\varepsilon_{A2}) < 2$).

In Fig. 5 we present the dependence of Andreev transmittance as a function of QD₂ energy for different values of inter-dot tunneling amplitude t_{12} and for coupling parameter Γ_{S2} . For $t_{12} = 0$ and $\Gamma_{S2} = 0$ (Fig. 5 (a)) the transmittance is independent of ε_2 . The non-zero value of

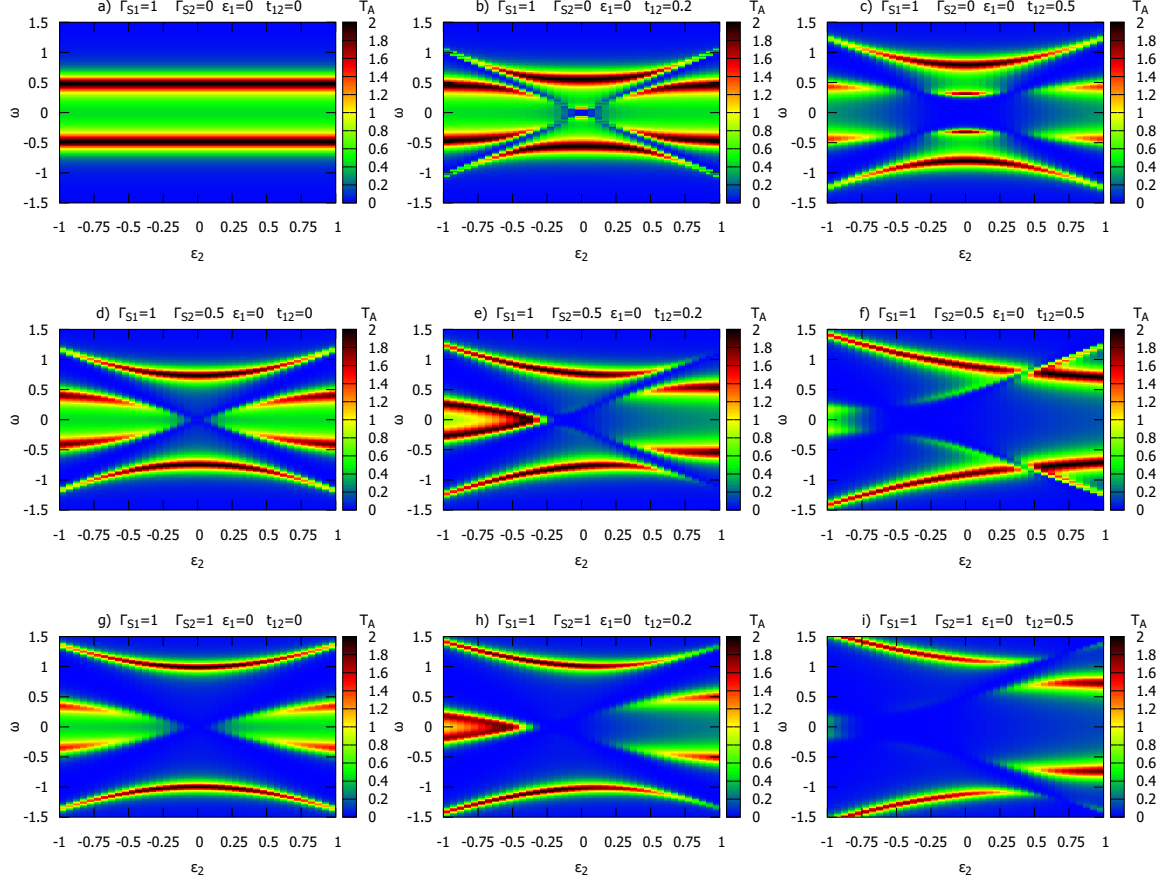


FIG. 5. The Andreev transmittance as a function of the QD₂ energy and for different values of the inter-dot tunneling amplitude t_{12} and coupling parameter Γ_{S2} . Other parameters are $\varepsilon_1 = 0$, $\Gamma_{S1} = 1$ and $\Gamma_N = 0.25$.

t_{12} or Γ_{S2} (Figs 5 (b)-(i)) causes that T_A is ε_2 dependent. For almost all values of ε_2 we obtain four resonances of Andreev transmittance.

For $t_{12} \neq 0$ and $\Gamma_{S2} = 0$ (i.e. for a T-shape configuration [4, 8]) or for $t_{12} = 0$ and $\Gamma_{S2} \neq 0$ (i.e. without direct coupling between QDs) we obtain $T_A(\omega, \varepsilon_2) = T_A(\omega, -\varepsilon_2)$ (see Figs 5 (b)-(c) and Figs 5 (d), (g), respectively). In the case of $t_{12} \neq 0$ and $\Gamma_{S2} = 0$ the zero value of Andreev transmittance is obtained for $\omega = \pm\varepsilon_2$ ($T_A(\varepsilon_2) = T_A(-\varepsilon_2) = 0$). One can see that the clear four resonances of Andreev transmittance are visible for any value of ε_2 (Figs 5 (b)-(c)). For $t_{12} \neq 0$ and $\Gamma_{S2} \neq 0$ (Figs 5 (e)-(f), (h)-(i)) the dependence $T_A(\omega, \varepsilon_2)$ is not symmetrical with respect to $\varepsilon_2 = 0$. For small values of t_{12} , the inner Andreev resonances come close to each other and, in effect, one obtains with properly chosen $\varepsilon_2 < 0$, one very strong peak of transmittance, close to 2, for $\omega = 0$.

The formation of a strong peak for $T_A(\omega = 0, \varepsilon_2)$ is of great importance for the zero-bias Andreev conductance $G_A = \partial I_N / \partial V|_{V \rightarrow 0}$. In Fig. 6 we show the dependence of G_A as a function of QD₂ energy for different values of inter-dot tunneling amplitude t_{12} . We have used the

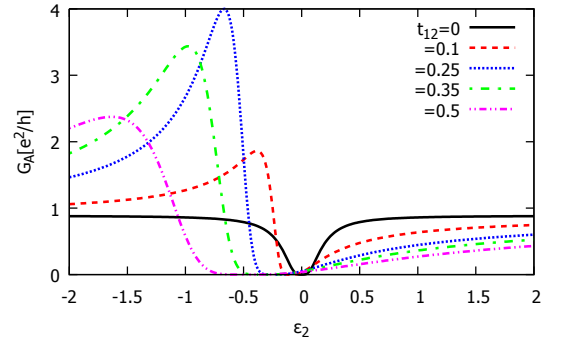


FIG. 6. The zero-bias Andreev conductance as a function of the QD₂ energy and for different values of the inter-dot tunneling amplitude t_{12} . Other parameters are $\varepsilon_1 = 0$, $\Gamma_{S1} = 1$ and $\Gamma_N = 0.25$.

symmetric coupling of QDs with SC lead, $\Gamma_{S1} = \Gamma_{S2} = 1$. For $\varepsilon_2 < 0$ and properly chosen value of t_{12} , we obtain the maximum value of $G_A = 4e^2/h$. For $\varepsilon_2 = -t_{12}$ we obtain $G_A = 0$.

These results can be compared to the zero-bias An-

dreev conductance results obtained for the N-QD-SC system which is coupled with the topological nanowire hosting Majorana modes (Majorana nanowire) [47, 48]. In such a system, for long Majorana nanowire, the optimal value of zero-bias conductance G_A is equal to $1/4$ of the quantum dot's conductance without the coupling with Majorana wire, $G_A|_{t_M \neq 0} = \frac{1}{4} G_A|_{t_M=0}$ [48]. In the case of QD₁ – QD₂ coupling, there occurs the total reduction of conductance, $G_A = 0$. It can be stated that only a fractional reduction of the zero-bias conductance testifies to the fractional fermion character of the Majorana mode. The measurement of the zero-bias Andreev conductance can be treated as the method which allows us to distinguish between the coupling of a QD with the Majorana nanowire (which is characterized by the fractional reduction of G_A) and the coupling of a QD with the second QD (where $G_A = 0$).

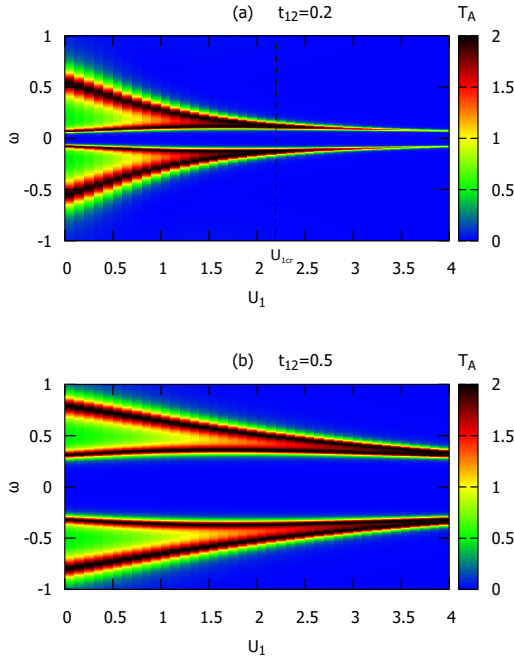


FIG. 7. The Andreev transmittance as a function of energy ω and the QD₁ Coulomb interaction U_1 for different values of the inter-dot tunneling amplitude t_{12} . Other parameters are $\varepsilon_1 = -U_1/2$, $\varepsilon_2 = 0$, $\Gamma_{S1} = 1$, $\Gamma_{S2} = 0$ and $\Gamma_N = 0.25$. The black dashed line marks U_{1cr} - see the text.

C. The influence of Coulomb interaction

The Coulomb interaction is very important, taking into account the spectral and transport properties of a quantum dot connected to the SC and metallic leads [34, 45, 49–53]. For the systems with a weak coupling of QD with metallic lead, the increase of Coulomb interaction causes the quantum phase transition between the (spin-less) BCS-like singlet and the (spin-full) dou-

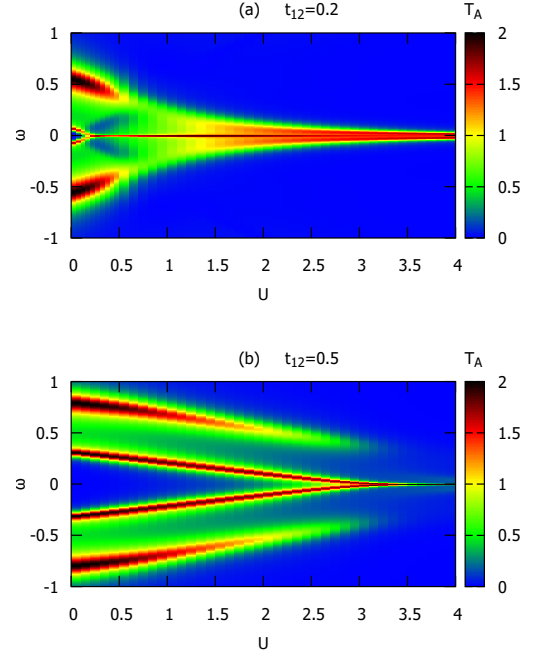


FIG. 8. The Andreev transmittance as a function of energy ω and the Coulomb interaction $U_1 = U_2 = U$ for different values of the inter-dot tunneling amplitude t_{12} . Other parameters are $\varepsilon_1 = -U/2$, $\varepsilon_2 = -U/2$, $\Gamma_{S1} = 1$, $\Gamma_{S2} = 0$ and $\Gamma_N = 0.25$.

blet configurations. This transition takes place for the values of Coulomb interaction close to the QD-SC coupling constant, Γ_S . For $U < \Gamma_S$ one observes the pair of Andreev peaks in the spectral function. The increase of U interaction causes the split of Andreev peaks, which give rise to the quasi-particle branches $\pm U/2 \pm E_d$, where $E_d = \sqrt{(\varepsilon + U/2)^2 + \Gamma_S^2/4}$. The inner low energy peaks approach each other, and for $U > \Gamma_S$ we obtain the strong, central Kondo peak for $\omega = 0$ and two Hubbard peaks near ε and $\varepsilon + U$.

The Coulomb interaction also modifies the Andreev transmittance of the N-QD-SC system. For $U < \Gamma_S$ we obtain two transmittance peaks. The increase of U values close to Γ_S causes the connection of these peaks to one central peak. For $U > \Gamma_S$ the disappearance of transmittance's central peak occurs.

Now, we will analyze the influence of the Coulomb interaction on the transport properties of a N-DQD-SC system using the second-order perturbation theory [48]. In our analysis we will consider two cases: (i) the Coulomb interaction exists only for QD₁ electrons ($U_1 \neq 0$ and $U_2 = 0$); (ii) the Coulomb interaction exists for both quantum dots ($U_1 = U_2 = U \neq 0$). Additionally, we will focus on the particle-hole symmetry case, i.e. when $\varepsilon_1 = -U_1/2$ and $\varepsilon_2 = -U_2/2$. In the first case, we will assume that the N – QD₁ – SC system, consisted of correlated QD₁ with $U_1 \neq 0$, is additionally connected to the uncorrelated QD₂. In fig. 7 we show the dependence

of $T_A(\omega)$ as a function of U_1 for different values of the inter-dot tunneling amplitude t_{12} . For all values of U_1 we obtain $T_A(0) = 0$. This result shows that a competition between the Fano and Kondo effects does not allow for the formation of the central Kondo peak for large values of U_1 interaction. The increase of U_1 interaction causes that the Andreev peaks ε_{A1} and ε_{A2} are getting closer but they will never connect each other. The location of ε_{A3} and ε_{A4} Andreev peaks, related to the proximity effect on QD₂, slightly shifts when the U_1 interaction increases. With properly selected value of $U_1 = U_{1cr}$ interaction, the overlap of ε_{A1} and ε_{A3} , and also ε_{A2} and ε_{A4} peaks occur, and as a result, for $U_1 > U_{1cr}$, we observe two narrowing peaks. The value of U_{1cr} increases as the t_{12} increases. In this case, the Fano-type resonance plays the dominant role.

Now, we will show the influence of the Coulomb interaction on the Andreev transmittance in a $U_1 = U_2 = U$ case (see Fig. 8). In this case, the increase of the Coulomb interaction causes that $T_A(0) \neq 0$ for all values of $U \neq 0$. Additionally, one can see that the Andreev peaks are getting closer to each other. For large values of t_{12} and U interactions, the Andreev peaks localized near ε_{A1} and ε_{A2} disappear, while the peaks localized near ε_{A3} and ε_{A4} are still visible.

IV. CONCLUSIONS

We have analyzed the spectral density and the transport properties of a double quantum dot. Both dots were coupled to a superconducting lead, while only one of them (QD₁) was coupled to the metallic lead. The coupling of both quantum dots with SC lead allows for direct

transport of the Cooper pair to the SC lead through one of two quantum dots and for a crossed transport via both quantum dots simultaneously.

The shape of spectral densities of quantum dots strongly depends on the coupling between QD₂ and SC lead. For $\Gamma_{S2} = 0$, the spectral densities of quantum dots show the existence of two pairs of Andreev resonances. Additionally, we obtain the Fano dip near $\omega = \varepsilon_2$.

The non-zero coupling of QD₂ with SC lead causes the extinction of the inner Andreev resonances. Additionally, $\Gamma_{S2} \neq 0$ causes the vanishing of the Fano dip. In the case of $\Gamma_{S2} = \Gamma_{S1}$ and $\varepsilon_1 = \varepsilon_2$, we obtain a three-center structure of spectral density consisting of one pair of Andreev resonances and a strong resonance peak near $\varepsilon_2 + t_{12}$.

For $\Gamma_{S2} = 0$, the Andreev transmittance shows one pair of broad peaks localized near ε_{A1} and ε_{A2} , and narrow resonances near ε_{A3} and ε_{A4} . In this case, the Andreev transmittance shows the Fano dip near $\pm\varepsilon_2$.

The non-zero value of Γ_{S2} causes the extinction of the inner Andreev transmittance resonances. In this case, the Fano dip are still visible, but its location depends on ε_2 , Γ_{S1} , Γ_{S2} and t_{12} . The level of QD₂ and t_{12} allows for strong modification of the zero-bias Andreev conductance value, G_A . For $\varepsilon_2 + t_{12} = 0$ we obtain the total reduction of G_A , while for properly selected values of ε_2 and t_{12} we can obtain very high values of G_A near $4e^2/h$.

ACKNOWLEDGMENTS

This project has been supported by the Center for Innovation and Transfer of Natural Sciences and Engineering Knowledge of Rzeszów University.

-
- [1] T.-S. Kim and S. Hershfield, "Suppression of current in transport through parallel double quantum dots," *Phys. Rev. B* **63**, 245326 (2001).
 - [2] P. S. Cornaglia and D. R. Grempel, "Strongly correlated regimes in a double quantum dot device," *Phys. Rev. B* **71**, 075305 (2005).
 - [3] R. Žitko and J. Bonča, "Enhanced conductance through side-coupled double quantum dots," *Phys. Rev. B* **73**, 035332 (2006).
 - [4] Y. Tanaka, N. Kawakami, and A. Oguri, "Andreev transport through side-coupled double quantum dots," *Phys. Rev. B* **78**, 035444 (2008).
 - [5] S. Sasaki, H. Tamura, T. Akazaki, and T. Fujisawa, "Fano-Kondo interplay in a side-coupled double quantum dot," *Phys. Rev. Lett.* **103**, 266806 (2009).
 - [6] R. Žitko, "Fano-Kondo effect in side-coupled double quantum dots at finite temperatures and the importance of two-stage Kondo screening," *Phys. Rev. B* **81**, 115316 (2010).
 - [7] I. L. Ferreira, P. A. Orellana, G. B. Martins, F. M. Souza, and E. Vernek, "Capacitively coupled double quantum dot system in the Kondo regime," *Phys. Rev. B* **84**, 205320 (2011).
 - [8] J. Barański and T. Domański, "Fano-type interference in quantum dots coupled between metallic and superconducting leads," *Phys. Rev. B* **84**, 195424 (2011).
 - [9] J. Barański and T. Domański, "Decoherence effect on Fano line shapes in double quantum dots coupled between normal and superconducting leads," *Phys. Rev. B* **85**, 205451 (2012).
 - [10] Y. Tanaka, N. Kawakami, and A. Oguri, "Crossover between two different Kondo couplings in side-coupled double quantum dots," *Phys. Rev. B* **85**, 155314 (2012).
 - [11] E. C. Siqueira and G. G. Cabrera, "Magnetoresistance and transistor-like behavior of a double quantum-dot via crossed Andreev reflections," *Journal of Applied Physics* **111**, 113905 (2012).
 - [12] A.M. Calle, M. Pacheco, and P.A. Orellana, "Fano effect and Andreev bound states in T-shape double quantum dots," *Phys. Letters A* **377**, 1474 – 1478 (2013).
 - [13] L. G. G. V. Dias da Silva, E. Vernek, K. Ingersent, N. Sandler, and S. E. Ulloa, "Spin-polarized conductance in double quantum dots: Interplay of Kondo, Zeeman, and interference effects," *Phys. Rev. B* **87**, 205313

- (2013).
- [14] K. P. Wójcik and I. Weymann, “Perfect spin polarization in T-shaped double quantum dots due to the spin-dependent Fano effect,” *Phys. Rev. B* **90**, 115308 (2014).
 - [15] J. Barański and T. Domański, “Fano-type resonances induced by a boson mode in Andreev conductance,” *Chinese Physics B* **24**, 17304 (2015).
 - [16] K. P. Wójcik and I. Weymann, “Two-stage Kondo effect in T-shaped double quantum dots with ferromagnetic leads,” *Phys. Rev. B* **91**, 134422 (2015).
 - [17] R. Žitko, “Numerical subgap spectroscopy of double quantum dots coupled to superconductors,” *Phys. Rev. B* **91**, 165116 (2015).
 - [18] K. P. Wójcik and I. Weymann, “Thermopower of strongly correlated T-shaped double quantum dots,” *Phys. Rev. B* **93**, 085428 (2016).
 - [19] A. M. Calle, M. Pacheco, G. B. Martins, V. M. Apel, G. A. Lara, and P. A. Orellana, “Fano-Andreev effect in a T-shape double quantum dot in the Kondo regime,” *J. Phys.: Condens. Matter* **29**, 135301 (2017).
 - [20] K. Wrześniewski and I. Weymann, “Kondo physics in double quantum dot based Cooper pair splitters,” *Phys. Rev. B* **96**, 195409 (2017).
 - [21] P. Busz, D. Tomaszewski, and J. Martinek, “Spin correlation and entanglement detection in Cooper pair splitters by current measurements using magnetic detectors,” *Phys. Rev. B* **96**, 064520 (2017).
 - [22] I. Weymann, R. Chirla, P. Trocha, and C. Moca, “SU(4) Kondo effect in double quantum dots with ferromagnetic leads,” *Phys. Rev. B* **97**, 085404 (2018).
 - [23] K. P. Wójcik and I. Weymann, “Interplay of the Kondo effect with the induced pairing in electronic and caloric properties of T-shaped double quantum dots,” *Phys. Rev. B* **97**, 235449 (2018).
 - [24] M. O. Assunção, G. S. Diniz, L. Sanz, and F. M. Souza, “Autler-Townes doublet observation via a Cooper-pair beam splitter,” *Phys. Rev. B* **98**, 075423 (2018).
 - [25] K. P. Wójcik and I. Weymann, “Nonlocal pairing as a source of spin exchange and Kondo screening,” *Phys. Rev. B* **99**, 045120 (2019).
 - [26] X.-Q. Wang, S.-F. Zhang, Y. Han, and W.-J. Gong, “Fano-Andreev effect in a parallel double quantum dot structure,” *Phys. Rev. B* **100**, 115405 (2019).
 - [27] P. Trocha and J. Barański, “Spin-polarized Andreev transport influenced by Coulomb repulsion through a two-quantum-dot system,” *Phys. Rev. B* **89**, 245418 (2014).
 - [28] J. Barański, T. Zienkiewicz, M. Barańska, and K. J. Kapcia, “Anomalous Fano resonance in double quantum dot system coupled to superconductor,” *Sci. Rep.* **10**, 2881 (2020).
 - [29] R. Shang, H.-O. Li, G. C., G. Yu, M. Xiao, T. Tu, G.-C. Guo, H. Jiang, A. M. Chang, and G.-P. Guo, “Observation of the Kondo effect in a quadruple quantum dot,” *Phys. Rev. B* **91**, 245102 (2015).
 - [30] R. N. Shang, T. Zhang, G. Cao, H.-O. Li, M. Xiao, G.-C. Guo, and G.-P. Guo, “Direct observation of the orbital spin Kondo effect in gallium arsenide quantum dots,” *Phys. Rev. B* **97**, 085307 (2018).
 - [31] J. Kondo, “Resistance minimum in dilute magnetic alloys,” *Progress of Theoretical Physics* **32**, 37 (1964).
 - [32] U. Fano, “Effects of configuration interaction on intensities and phase shifts,” *Phys. Rev.* **124**, 1866–1878 (1961).
 - [33] A. F. Andreev, “The thermal conductivity of the intermediate state in superconductors,” *J. Exp. Theor. Phys.* **19**, 1228 (1964).
 - [34] A. Martín-Rodero and A. Levy Yeyati, “Josephson and Andreev transport through quantum dots,” *Advances in Physics* **60**, 899 (2011).
 - [35] S. Nadj-Perge, I. K. Drozdov, J. Li, H. Chen, S. Jeon, J. Seo, A. H. MacDonald, B. A. Bernevig, and A. Yazdani, “Observation of Majorana fermions in ferromagnetic atomic chains on a superconductor,” *Science* **346**, 602 (2014).
 - [36] R. Pawlak, M. Kisiel, J. Klinovaja, T. Maier, S. Kawai, T. Glatzel, D. Loss, and E. Meyer, “Probing atomic structure and Majorana wave-functions in mono-atomic Fe-chains on superconducting Pb-surface,” *npj Quantum Info* **2**, 16035 (2016).
 - [37] S. Jeon, Y. Xie, J. Li, Z. Wang, B. A. Bernevig, and A. Yazdani, “Distinguishing a Majorana zero mode using spin-resolved measurements,” *Science* **358**, 772 (2017).
 - [38] M. Ruby, B. W. Heinrich, Y. Peng, F. von Oppen, and K. J. Franke, “Exploring a proximity-coupled Co chain on Pb(110) as a possible Majorana platform,” *Nano Letters* **17**, 4473–4477 (2017).
 - [39] H. Kim, A. Palacio-Morales, T. Posske, L. Rózsa, K. Palotás, L. Szunyogh, M. Thorwart, and R. Wiesendanger, “Toward tailoring Majorana bound states in artificially constructed magnetic atom chains on elemental superconductors,” *Sci. Adv.* **4**, eaar5251 (2018).
 - [40] C.-X. Liu, J. D. Sau, and S. Das Sarma, “Distinguishing topological Majorana bound states from trivial Andreev bound states: Proposed tests through differential tunneling conductance spectroscopy,” *Phys. Rev. B* **97**, 214502 (2018).
 - [41] A. V. Rozhkov and Daniel P. Arovas, “Interacting-impurity Josephson junction: Variational wave functions and slave-boson mean-field theory,” *Phys. Rev. B* **62**, 6687–6691 (2000).
 - [42] J. Eldridge, M. G. Pala, M. Governale, and J. König, “Superconducting proximity effect in interacting double-dot systems,” *Phys. Rev. B* **82**, 184507 (2010).
 - [43] A.-P. Jauho, N. S. Wingreen, and Y. Meir, “Time-dependent transport in interacting and noninteracting resonant-tunneling systems,” *Phys. Rev. B* **50**, 5528–5544 (1994).
 - [44] Q.-F. Sun, J. Wang, and T.-h. Lin, “Control of the supercurrent in a mesoscopic four-terminal Josephson junction,” *Phys. Rev. B* **62**, 648–660 (2000).
 - [45] Y. Yamada, Y. Tanaka, and N. Kawakami, “Interplay of kondo and superconducting correlations in the nonequilibrium Andreev transport through a quantum dot,” *Phys. Rev. B* **84**, 075484 (2011).
 - [46] G. Deutscher, “Andreev-Saint-James reflections: A probe of cuprate superconductors,” *Rev. Mod. Phys.* **77**, 109–135 (2005).
 - [47] J. Barański, A. Kobińska, and T. Domański, “Spin-sensitive interference due to Majorana state on the interface between normal and superconducting leads,” *J. Phys.: Condens. Matter* **29**, 075603 (2017).
 - [48] G. Górski, J. Barański, I. Weymann, and T. Domański, “Interplay between correlations and Majorana mode in proximitized quantum dot,” *Sci. Rep.* **8**, 15717 (2018).
 - [49] Y. Tanaka, N. Kawakami, and A. Oguri, “Numerical renormalization group approach to a quantum dot coupled to normal and superconducting leads,” *J. Phys. Soc. Japan* **76**, 074701 (2007).
 - [50] R. S. Deacon, Y. Tanaka, A. Oiwa, R. Sakano,

- K. Yoshida, K. Shibata, K. Hirakawa, and S. Tarucha, “Kondo-enhanced Andreev transport in single self-assembled InAs quantum dots contacted with normal and superconducting leads,” *Phys. Rev. B* **81**, 121308 (2010).
- [51] R. Žitko, J. Soo Lim, R. López, and R. Aguado, “Shiba states and zero-bias anomalies in the hybrid normal-superconductor Anderson model,” *Phys. Rev. B* **91**, 045441 (2015).
- [52] T. Domański, I. Weymann, M. Barańska, and G. Górski, “Constructive influence of the induced electron pairing on the Kondo state,” *Sci. Rep.* **6**, 23336 (2016).
- [53] X.-J. Hao, H.-O. Li, T. Tu, C. Zhou, G. Cao, G.-C. Guo, G.-P. Guo, W. Y. Fung, Z. Ji, and W. Lu, “Andreev tunneling enhanced by Coulomb oscillations in superconductor-semiconductor hybrid Ge/Si nanowire devices,” *Phys. Rev. B* **84**, 195448 (2011).